EngOpt 2012 - International Conference on Engineering Optimization
Rio de Janeiro, Brazil, 1-5 July 2012.

Exploring the use of Adjoint Methods for Detailed Sensitivity Analysis on Turbomachinery

Andre C. Marta* **and Sriram Shankaran†**

∗ Instituto Superior Técnico, Lisboa, Portugal, andre.marta@ist.utl.pt
† Global Research Center, General Electric, Niskayuna, USA, shankaran@ge.com

Abstract

During the last decade, significant progress has been made in the field of optimization using high-fidelity models. The increased use of adjoint methods has allowed the computation of sensitivity information, required by gradient-based optimizers, in a very efficient manner. In terms of fluid dynamics, while the first applications were focused on aerodynamic shape design, recent approaches to the development of adjoint solvers, namely with the use of automatic differentiation tools, have made possible to extend their capabilities far beyond that. The present paper briefly describes a discrete adjoint method implementation for a generic CFD solver and lays down the steps to estimate sensitivities of functions of interest with respect to any variables handled by the flow solver. The applications presented are based on turbomachinery blade design problems. Two different capabilities are illustrated: one more traditional geared toward shape optimization that focuses on estimating gradients of some turbomachinery aerodynamic performance parameters with respect to blade geometry, and another more innovative geared toward estimating the effect of the inlet or exit boundary conditions on some aerothermal performance parameters. The computational cost required by this method in terms of CPU time is considerably reduced compared to the popular finite-difference method, at the expense of a more complex implementation. The detailed sensitivity information obtained is discussed from a designer perspective. Other possible applications of adjoint methods are listed and their development implications are also described.

Keywords: Turbomachinery, Shape, Boundary conditions, Optimization, Adjoint method, Sensitivity.

1 Introduction

In the last decades, turbomachinery design has greatly benefited with the use of high-fidelity computational tools, including but not limited to aerodynamic, aerothermal, structural and dynamic analyses. Of particular interest is the expanding role of computational fluid dynamic (CFD) simulations, departing from the conventional simulation analysis to advanced design optimization tasks.

When it comes to optimization, it is well known that gradient-based algorithms, whenever possible to be used, are the most efficient in terms of computational resources required to drive the solution to its optimal. However, derivatives of the functions of interest need to be provided to such class of algorithms. This, by itself, can pose a problem as most sensitivity analysis methods can become too costly when the number of optimization variables is very large. A good example are finite-differences, whose computational cost scales linearly with the number of variables.

For problems when the number of variables greatly exceeds the number of functions, the adjoint method is the best-suited approach to efficiently estimate function gradients since the cost involved in calculating sensitivities is practically independent of the number of design variables.

The first application of the adjoint method to CFD is credited to Pironneau [1] back in 70's. Since then, much progress has been made extending its application to aeronautical problems, ranging from airfoils [2] to complete wings [3], from external [4] to internal flows [5], and even multi-stage turbomachines [6] and robust optimization [7].

While these applications were on shape optimization, that is, where the design variables were shape parameters, and where the functions of interest were of aerodynamic nature, such as wing drag or blade efficiency, the adjoint method can be extended to other classes of problems in a straightforward manner.

In this paper, a generic derivation of the adjoint equations is provided and two distinct applications are presented: the first being a conventional aerodynamic problem using wall shape design variables, while the second is an aerothermal problem using inlet or exit boundary conditions.

2 Background

The underlying theory of design optimization and adjoint-based sensitivity analysis using high-fidelity CFD are presented in this section. First, the design problem is posed in non-linear programming form, then the flow governing equations are presented and their corresponding adjoint equations are derived, followed by the adjoint-based gradients expressions. Finally, a possible gradient-based optimization framework is discussed.

2.1 Generic Design Problem

The design of any turbomachinery component can be mathematically formulated as an optimization problem. In generic terms, this problem can be cast in non-linear programming (NLP) form as

$$\begin{aligned} \text{minimize} \quad & f(\boldsymbol{\alpha}, \boldsymbol{\omega}(\boldsymbol{\alpha})) \\ \text{w.r.t.} \quad & \boldsymbol{\alpha} \\ \text{subject to} \quad & \mathcal{R}(\boldsymbol{\alpha}, \boldsymbol{\omega}(\boldsymbol{\alpha})) = 0 \\ & \boldsymbol{c}(\boldsymbol{\alpha}, \boldsymbol{\omega}(\boldsymbol{\alpha})) = 0\,, \end{aligned} \tag{1}$$

where f stands for the objective (or cost) function, $\boldsymbol{\alpha}$ is the vector of design variables and $\boldsymbol{\omega}$ is the state solution, which is typically of function of the design variables, and $\boldsymbol{c} = 0$ represents additional constraints that may or may not involve the state solution. For the particular case of a CFD design problem, $\boldsymbol{\omega}$ is the flow solution, and the additional constraint $\mathcal{R} = 0$ represents the flow governing equations, which means that the solution must always obey the flow physics.

In turbomachinery design, examples of functions of interest, either objective f or constraints c can be blade efficiency, pressure ratio, mass flow or surface temperature. The design variables, that represent the tuning parameters, can be some form of blade shape control, such as blade stagger, camber angle and thickness distributions, axial and radial stacking. Other possibility of design variables is to consider the boundary conditions of the governing equations themselves. An example could be the inlet total temperature or turbulence intensity radial profiles, assuming one as some degree of control over these.

It is of paramount importance to the designer to assess the sensitivity of the functions of interest with respect to the tuning parameters, that is to say, a detailed sensitivity analysis ought to be conducted so that estimates to $\mathrm{d}f/\mathrm{d}\boldsymbol{\alpha}$ and $\mathrm{d}c_i/\mathrm{d}\boldsymbol{\alpha}$ are obtained. Moreover, in case the NLP problem (1) is to be solved numerically using a gradient-based optimizer, these sensitivities are necessary and must be evaluated in an accurate and timely manner.

2.2 Flow Governing Equations

The governing equations used in the present work are the Reynolds-Averaged Navier–Stokes (RANS) equations. In conservation form, the Navier–Stokes system of equations may be written in index notation as

$$\frac{\partial \rho}{\partial t} + \frac{\partial}{\partial x_j}\left(\rho u_j\right) = 0\,, \tag{2a}$$

$$\frac{\partial}{\partial t}\left(\rho u_i\right) + \frac{\partial}{\partial x_j}\left(\rho u_i u_j + p\delta_{ij} - \tau_{ji}\right) = 0, \quad i = 1, 2, 3\,, \tag{2b}$$

$$\frac{\partial}{\partial t}\left(\rho E\right) + \frac{\partial}{\partial x_j}\left(\rho E u_j + p u_j - u_i \tau_{ij} + q_j\right) = 0\,, \tag{2c}$$

where ρ, u_i and E are respectively the density, mean velocity and total energy, τ_{ij} is the viscous stress and q_j is the heat flux. A turbulence model needs to be used to model the Reynolds stresses. In this paper, a two-equation turbulence model was used, in particular the $k-\omega$ model of Wilcox [8],

$$\frac{\partial}{\partial t}(\rho k) + \frac{\partial}{\partial x_j}(\rho k u_j) = \tau_{ij}\frac{\partial u_i}{\partial x_j} - \beta_k \rho k \omega + \frac{\partial}{\partial x_j}\left[\left(\mu + \sigma_k \frac{\rho k}{\omega}\right)\frac{\partial k}{\partial x_j}\right], \tag{3a}$$

$$\frac{\partial}{\partial t}(\rho\omega) + \frac{\partial}{\partial x_j}(\rho\omega u_j) = \frac{\gamma\omega}{k}\tau_{ij}\frac{\partial u_i}{\partial x_j} - \beta_\omega\rho\omega^2 + \frac{\partial}{\partial x_j}\left[\left(\mu + \sigma_\omega\frac{\rho k}{\omega}\right)\frac{\partial\omega}{\partial x_j}\right], \tag{3b}$$

where k is the turbulence kinetic energy and ω is the specific dissipation rate. The turbulent eddy viscosity is computed from $\mu_T = \rho k/\omega$ and the constants are $\gamma = 5/9$, $\beta_k = 9/100$, $\beta_\omega = 3/40$, $\sigma_k = 1/2$ and $\sigma_\omega = 1/2$. The effective viscosity used in the Navier–Stokes equations (2) is then computed as $\mu = \mu_m + \mu_T$, where μ_m is the molecular (laminar) viscosity.

In semi-discrete form, the RANS governing equations (2,3) can be expressed for a given computional cell n as

$$\frac{\mathrm{d}\boldsymbol{\omega}_n}{\mathrm{d}t} + \mathcal{R}_n(\boldsymbol{\omega}) = 0\,, \tag{4}$$

where $\boldsymbol{\omega} = (\rho, \rho\boldsymbol{u}, \rho E, \rho k, \rho\omega)^T$ is the vector of conservative variables and $\mathcal{R}$ is the residual with all of its components (inviscid, viscous and turbulent fluxes, boundary conditions and artificial dissipation) The unsteady term of Eq.(4) is dropped out since only the steady solution of the equation is of interest in this work.

2.3 Adjoint Equations

The derivation of the adjoint equations for systems of PDEs follows the work by Giles [9]. The adjoint equations of the flow Eq.(4) can be expressed as

$$\left[\frac{\partial\mathcal{R}}{\partial\boldsymbol{\omega}}\right]^T\boldsymbol{\psi} = \left[\frac{\partial f}{\partial\boldsymbol{\omega}}\right]^T, \tag{5}$$

where $\boldsymbol{\psi}$ is the adjoint state vector.

Once the adjoint solution is computed from Eq.(5), the gradient of the function of interest with respect to the design variables $\boldsymbol{\alpha}$ is easily obtained from a simple matrix-vector multiplication operation given by

$$\frac{\mathrm{d}f}{\mathrm{d}\boldsymbol{\alpha}} = \frac{\partial f}{\partial\boldsymbol{\alpha}} - \boldsymbol{\psi}^T\frac{\partial\mathcal{R}}{\partial\boldsymbol{\alpha}}\,. \tag{6}$$

It is important to highlight the dependence of the adjoint equation on the function of interest f. This implies solving Eq.(5) with a new right-hand side vector for each function of interest, that is, for the objective function f and constraints $\boldsymbol{c}$ in the optimization problem Eq.(1).

On the other hand, the computational cost of the total sensitivity Eq.(6) is almost independent of the number of design variables $\boldsymbol{\alpha}$, which is the feature that makes the adjoint method so attractive for gradient-based optimization involving a large number of variables and a few functions.

2.4 Optimization Framework

As already mentioned, the NLP problem in Eq.(1) can be solved using a gradient-based optimization algorithm.

Let $\boldsymbol{\alpha}$ denote the set of design parameters controlled by the optimizer. Using the set of values provided by the optimizer, the flow solver of Eq.(4) is run to compute the flow solution $\boldsymbol{\omega}$ and, using some post-processing, the functions of interest f or c are evaluated and passed back to the optimizer. Using the flow solution obtained by running the flow solver, the adjoint solution $\boldsymbol{\psi}$ corresponding to the functions of interest is then computed using the adjoint solver. Once the adjoint solution is evaluated from Eq.(5), the gradients of the functions of interest with respect to the design parameters are computed by Eq.(6), which implies a simple matrix-vector multiplication operation, and passed back to the optimizer. The function values and gradients are then used by the optimizer to find the search direction, along which a step is taken in the design space. The optimizer then loops though the described steps until the optimality criteria are satisfied.

The schematic of the adjoint-based optimization algorithm just described is illustrated in Fig. 1.

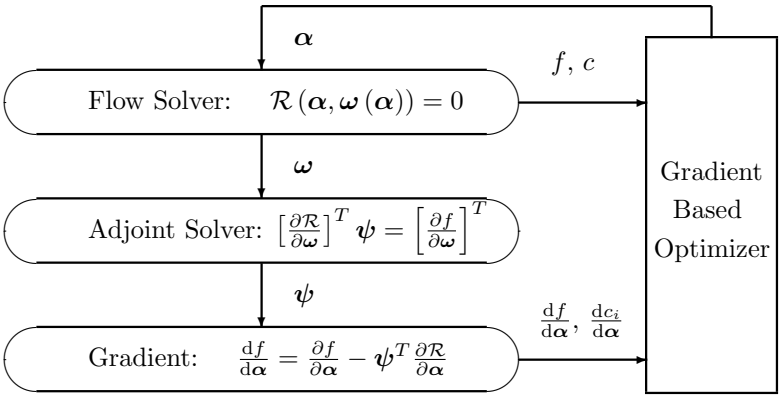

Figure 1: Schematic of the adjoint-based optimization algorithm.

In terms of computational cost, the flow and adjoint solvers are the two main blocks of the process, being the cost of the solution of the adjoint equations approximately the same as that of the solution of the flow governing equations, since both equations are of similar size and complexity.

The algorithm illustrated in Fig. 1 is rather simplistic. In practice, some additional pre- and post-processing steps need to be considered, like mesh generation and deformation, or even transformation of variables. For instance, if the desired design variables $\boldsymbol{\beta}$ are not handled explicitly by the flow solver, then it is necessary to derive the relation $\boldsymbol{\alpha} = \boldsymbol{\alpha}(\boldsymbol{\beta})$ and use the chain rule of differentiation to express the gradient of the function of interest with respect to the design variables as

$$\frac{\mathrm{d}f}{\mathrm{d}\boldsymbol{\beta}} = \frac{\mathrm{d}f}{\mathrm{d}\boldsymbol{\alpha}} \frac{\mathrm{d}\boldsymbol{\alpha}}{\mathrm{d}\boldsymbol{\beta}} \,. \tag{7}$$

The method used to evaluate the term $\frac{\mathrm{d}\boldsymbol{\alpha}}{\mathrm{d}\boldsymbol{\beta}}$ is problem dependent. If the relation expressed by Eq.(7) is known explicitly, even if in the form of a source code, then the adjoint method can again be used. In contrast, if that relation is given by some sort of a black box, such as a commercial CAD or mesh generator software, then most likely a finite-difference approximation has to be used.

3 Implementation

The legacy flow solver is briefly described and main properties of the corresponding adjoint solver are highlighted in this section.

3.1 Flow Solver

The flow solver used is an in-house developed code for the analysis of turbomachinery blade rows. It solves the RANS Eqs. (2,3) in multi-block, three-dimensional, structured grids, using the finite-volume technique, and supporting multi-processor execution.

As typical for most iterative CFD solvers, the residual calculation is done by looping through the discretized domain and accumulating the several fluxes and boundary conditions contributions in the residual $\mathcal{R}_n$ of each cell.

3.2 Adjoint Solver

The simple mathematical form of Eq.(5) can be very misleading since, depending on the approach, their numerical implementation can be quite complex, if derived by manual differentiation, or quite costly, if derived using finite-differences.

A discrete adjoint approach formulation was chosen because it can be applied to any set of governing equations, namely full RANS with turbulent adjoint terms, and it can treat arbitrary functions of

interest. In addition, the discrete approach allowed the use of automatic differentiation (AD) tools [10] in its derivation, considerably mitigating the cost of developing the adjoint solver.

This resulting hybrid approach follows the work of Marta [11]. It retains the accuracy of the adjoint methods, while it adds the ease of implementation of the automatic differentiation methods. The discrete adjoint solver was derived with the aid of an AD tool that was selectively applied to the CFD source code that handled the evaluations of the residual $\mathcal{R}$ and functions of interest f. That tool produced the routines that evaluate the entries of the partial derivative matrices $\partial\mathcal{R}/\partial\boldsymbol{\omega}$, $\partial f/\partial\boldsymbol{\omega}$, $\partial f/\partial\boldsymbol{\alpha}$ and $\partial\mathcal{R}/\partial\boldsymbol{\alpha}$ that are necessary to compute gradients in Eq.(6) using the adjoint solution from Eq.(5).

The sizes of the matrices involved in this process are

$$\frac{\partial\mathcal{R}}{\partial\boldsymbol{\omega}} \quad (N_\omega \times N_\omega) \ , \quad \frac{\partial f}{\partial\boldsymbol{\omega}} \quad (N_f \times N_\omega) \ , \quad \frac{\partial\mathcal{R}}{\partial\boldsymbol{\alpha}} \quad (N_\omega \times N_\alpha) \ , \quad \frac{\partial f}{\partial\boldsymbol{\alpha}} \quad (N_f \times N_\alpha) \ , \tag{8}$$

where N_f is the number of functions of interest, N_α is the number of design variables and N_ω is the size of the state vector. The size of the vector $\boldsymbol{\omega}$ depends on the number of governing equations, N_e (seven for RANS), and the number of cells of the computational mesh, N_c, that discretize the physical domain, according to the relation $N_\omega = N_e \times N_c$, which for the solution of a large problem is very large.

The details about the adjoint solver implementation and verification can be found in reference [5].

4 Results

This section demonstrates the capability of the adjoint method to estimate, accurately and in detail, the sensitivity of some functions of interest with respect to different design variables. It includes two distinct turbomachine blades: a high-pressure compressor rotor blade and a low-pressure turbine stator vane. For each test case, adjoint-based sensitivity information is computed for different functions of interest and design variables.

4.1 Compressor Rotor Blade

A transonic blade of a high-pressure compressor stage was used to demonstrate the capabilities of the adjoint solver handling grid coordinates as design variables.

The full wheel geometry is shown in Fig. 2(a). The close up of the blades is presented in Fig. 2(b), where the casing wall has been removed for visual clarity.

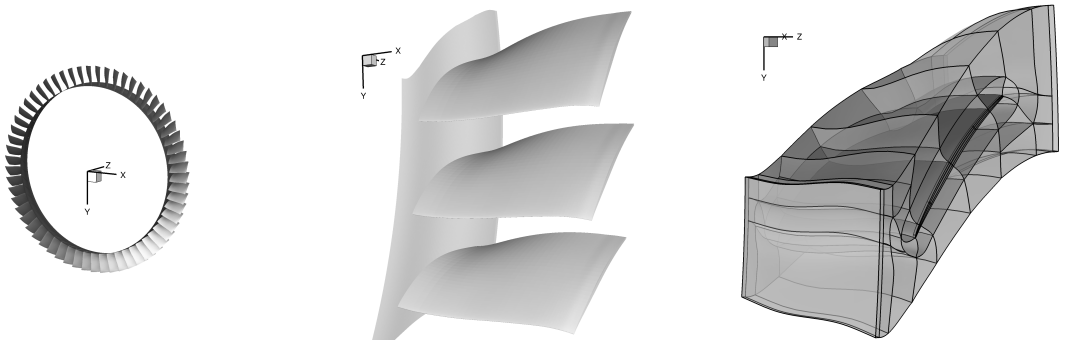

(a) Full wheel (b) Close up (c) Computational domain

Figure 2: Compressor rotor geometry.

The mesh generated has a OH-grid topology around the blade, reverting to H-grid topology further away from the blade, and a wall refinement leading to an average y^+ of 25. A total of 60 blocks were created, as shown in Fig. 2(c), totaling 1.2 million cells, and the simulations were run on a cluster using 32 processors.

The inlet boundary conditions were absolute tangential velocity fixed and pressure extrapolated from the interior. The exit static pressure was held fixed. All solid walls were considered impermeable with no-slip condition. The remaining faces were either block-to-block interfaces or periodic.

In this test case, the isentropic efficiency was used as function of interest f,

$$\eta = \frac{\left(P^{enth}_{ta\ exit}/P^{enth}_{ta\ inlet}\right)^{(\gamma-1)/\gamma} - 1}{(T^{mass}_{ta\ exit}/T^{mass}_{ta\ inlet}) - 1}, \tag{9}$$

where the superscripts $enth$, $mass$ and $area$ indicate an enthalpy, mass and area averaged quantities at the inlet or exit sections.

The coordinates of each computational grid node $(x, y, z)_n$ were assumed to be design variables, which meant a total of 3.6 million parameters (N_α).

Given that the full adjoint solution was used, seven adjoint variables, $(\rho, \rho u, \rho v, \rho w, \rho E, \rho k, \rho\omega)_{adj}$, were computed at each computational node, thus $N_\omega \approx 8.4$ million.

4.1.1 Flow and Adjoint Solutions

The contours of non-dimensional density on the hub and blade surface are shown in Fig. 3(a), where the flow goes in the positive z direction. The corresponding adjoint solution of the continuity equation for isentropic efficiency, setting $f = \eta$ in Eq.(5), is shown in Fig. 3(b).

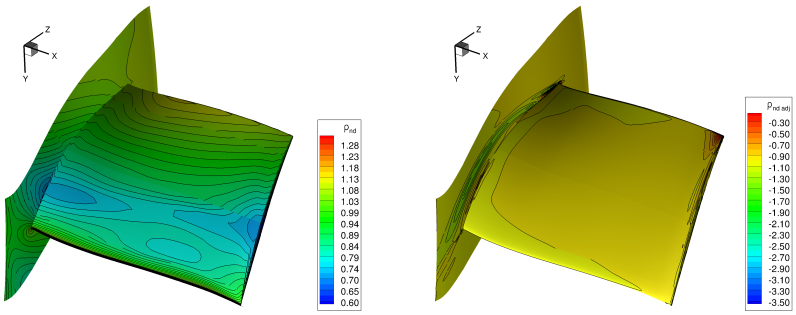

(a) Flow (b) Adjoint

Figure 3: Flow and adjoint solution for the compressor rotor blade.

The average inlet density and the average exit adjoint of the continuity equation were used as reference for the non-dimensionalization of the flow and adjoint solutions, respectively.

As typically found in adjoint solutions, the plot in Fig. 3(b) shows an adjoint flow some how reverse of the real flow. The wake emanates from the blade trailing edge as a consequence of the adjoint flow pointing in the negative direction. This is the result of the representation of the adjoint time τ as the negative of the physical time t as inferred from the derivation of the adjoint equations [9].

Further details on the interpretation of adjoint solutions cab be found in reference [12].

4.1.2 Adjoint-Based Gradients

The contours of the gradient of the compressor rotor blade efficiency with respect to each node of the grid coordinate components, $(x, y, z)_n$, evaluated using Eq.(6), are illustrated in Fig. 4 for the hub and blade surface nodes.

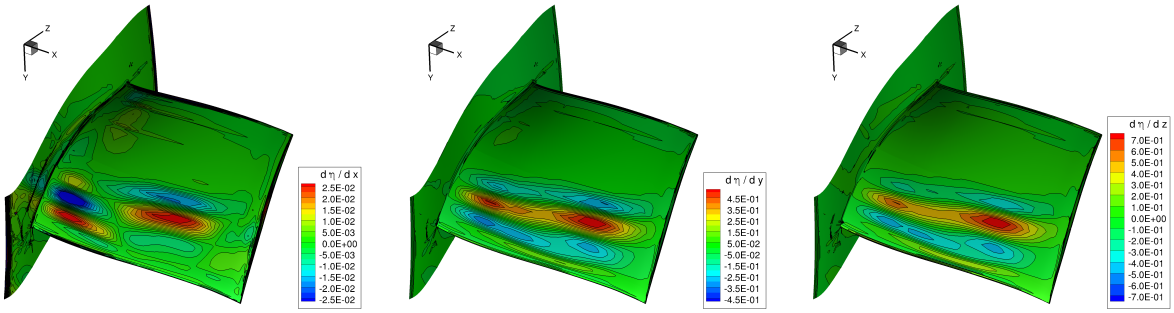

(a) $\mathrm{d}\eta/\mathrm{d}x$ (b) $\mathrm{d}\eta/\mathrm{d}y$ (c) $\mathrm{d}\eta/\mathrm{d}z$

Figure 4: Gradient of compressor rotor blade efficiency w.r.t. node coordinates.

The large values at the blade leading edge reveal how sensitive the machine performance is relative to this region. It is also possible to obtain the sensitivity of blade efficiency with respect to the radius r of the hub wall by combining the x and y components as

$$\frac{\mathrm{d}\eta}{\mathrm{d}r} = \frac{\mathrm{d}\eta}{\mathrm{d}x}\frac{\mathrm{d}x}{\mathrm{d}r} + \frac{\mathrm{d}\eta}{\mathrm{d}y}\frac{\mathrm{d}y}{\mathrm{d}r} = \frac{\mathrm{d}\eta}{\mathrm{d}x}cos(\theta) + \frac{\mathrm{d}\eta}{\mathrm{d}y}sin(\theta) \tag{10}$$

where θ is the tangential angle in cylindrical coordinates measured from the x to the y axis. This sensitivity is presented graphically in Fig. 5.

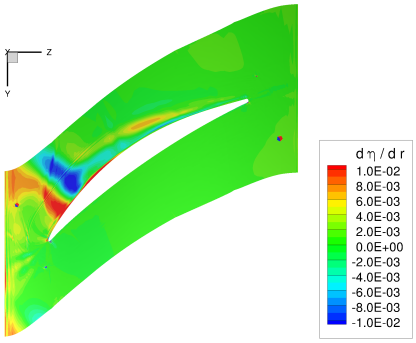

Figure 5: Gradient of compressor rotor blade efficiency w.r.t. hub radius.

The information contained in plots like the ones in Fig. 4 and Fig. 5 can be extremely valuable during blade shape design, even for the experienced designer. In this particular case, an increase in blade efficiency is expected by placing an elevation in the red region and a depression in the blue region of the hub wall. This technique of shaping the hub or casing walls are known as endwall contouring.

4.2 Turbine Stator Vane

A vane of a low-pressure turbine stage was used to demonstrate the capabilities of the adjoint solver handling inlet or exit boundary conditions as design variables.

Similarly to the previous test case, the full wheel geometry and a close up of the vane are shown in Fig. 6(a) and Fig. 6(b), respectively.

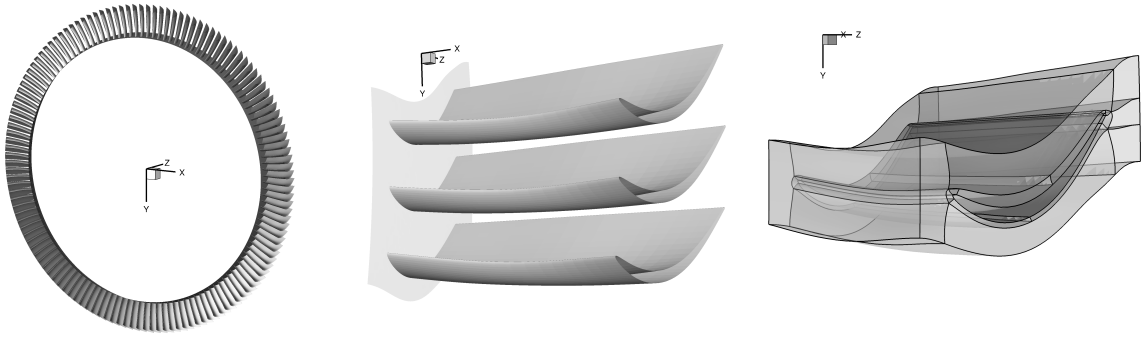

(a) Full wheel (b) Close up (c) Computational domain

Figure 6: Turbine stator geometry.

Being a stator blade, no tip gap had to be modeled and, as such, a considerably simpler mesh was generated. It was still an OH-grid around the blade, but only 15 blocks were needed, as shown in Fig. 6(c). A much coarser mesh was produced, totaling only 44 thousand cells, and the simulations were run on a workstation using 4 processors. The same type of boundary conditions as in test case 4.1 were used.

For this test case, the total temperature averaged over a user-specified wall surface was used as function of interest f,

$$T_{T\,avg} = \frac{\int_\Omega T_T \mathrm{d}\Omega}{\int_\Omega \mathrm{d}\Omega}\,, \tag{11}$$

where the superscript avg indicates an area averaged quantity at the specified wall surface Ω.

The results presented were obtained by specifying the pressure and suction vane sides as the surface Ω used to compute the area-averaged total temperature in Eq.(11).

The boundary conditions at the inlet plane were assumed to be design parameters, that is, the total pressure, total temperature, tangential velocity, radial and axial velocity cosines at each node of the 40×18 inlet grid plane nodes were considered variables. This totaled $N_\alpha = 3,600$ parameters.

4.2.1 Flow and Adjoint Solutions

The contours of non-dimensional density and adjoint solution of the continuity equation for area-averaged total temperature ($f = T_{T\,avg}$) on the vane surface are shown in Fig. 7(a) and Fig. 7(b), respectively.

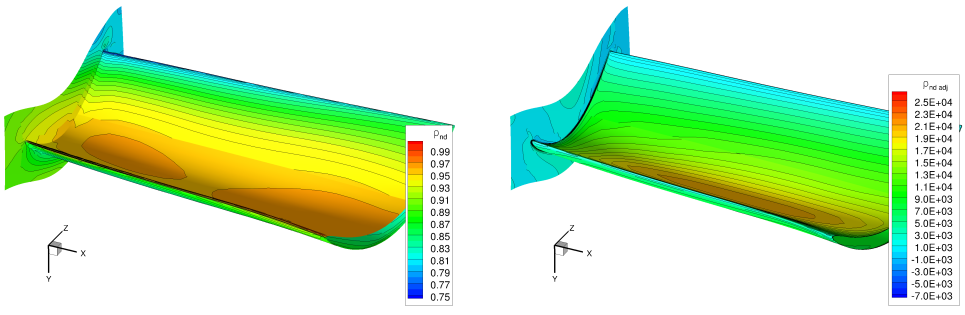

(a) Flow (b) Adjoint

Figure 7: Flow and adjoint solution for the turbine stator vane.

The reference values for non-dimensionalization were taken at the inlet and exit planes for the flow and adjoint states, respectively.

4.2.2 Adjoint-Based Gradients

The contours of the gradient of the area-averaged total temperature on the vane surface with respect to the boundary conditions at each node of the inlet grid are illustrated in Fig. 8.

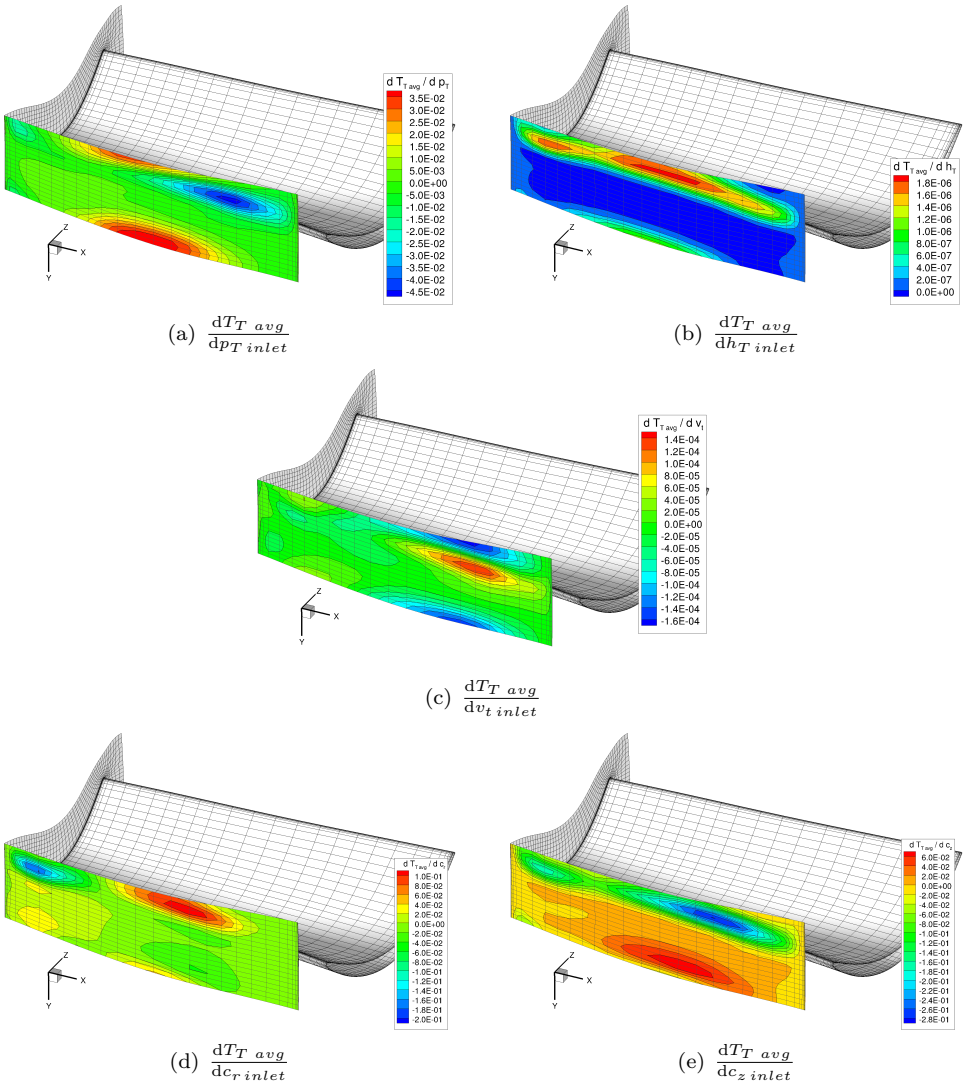

(a) $\frac{\mathrm{d}T_{T\ avg}}{\mathrm{d}p_{T\ inlet}}$ (b) $\frac{\mathrm{d}T_{T\ avg}}{\mathrm{d}h_{T\ inlet}}$

(c) $\frac{\mathrm{d}T_{T\ avg}}{\mathrm{d}v_{t\ inlet}}$

(d) $\frac{\mathrm{d}T_{T\ avg}}{\mathrm{d}c_{r\ inlet}}$ (e) $\frac{\mathrm{d}T_{T\ avg}}{\mathrm{d}c_{z\ inlet}}$

Figure 8: Gradient of turbine vane averaged total temperature w.r.t. inlet boundary conditions.

The red contours in Fig. 8(b) denote the region whose increase in total enthalpy would lead to an increase in the vane averaged total temperature; this happens because enthalpy is directly related to temperature and because the flow at that inlet region will later directly impinge the vane. The other plots in Fig. 8, even though as not straightforward to interpret, can also be used by the turbine designer to help him properly match different stages while complying with heat transfer constraints.

5 Conclusions

The adjoint method was used to compute sensitivities of some performance metrics with respect to different parameters in turbomachinery blades. Two test cases were used to demonstrate different kind of functions of interest and design variables. The functions included an aerodynamic metric – isentropic efficiency — and an aerothermal metric — averaged total temperature. The design variables included

shape parameters, in the form of grid coordinates, and inlet boundary conditions. The shear amount of information obtained was only possible thanks to the adjoint method. It would be virtually impossible to use any other type of sensitivity analysis method to handle such a large number of design variables.

Given the proliferation of adjoint methods, in part due to new techniques to develop adjoint solvers for legacy flow solvers, the designers can now be offered a totally new level of information with their CFD simulations. The detailed flow analysis can now be complemented with an equally detailed sensitivity analysis, using any kind of function of interest f and design variable α, as expressed in Eq.(5) and Eq.(6). The next challenge will be on how to properly embed such wealthy data into the current design process. While the sensitivity analysis can be used to provide physical insight to the designer in terms of quality and robustness of a given blade design, as demonstrated in the included test cases, it can also prove to be an irreplaceable block in a gradient-based optimization framework, as depicted in Fig. 1.

Acknowledgements

The authors are thankful to General Electric for giving permission to publish this paper.

References

[1] O. Pironneau. On optimum design in fluid mechanics. *Journal of Fluid Mechanics*, 64:97–110, 1974.

[2] A. Jameson. Aerodynamic design via control theory. *Journal of Scientific Computing*, 3(3):233–260, September 1988.

[3] A. Jameson, N. A. Pierce, and L. Martinelli. Optimum aerodynamic design using the Navier–Stokes equations. In *Theoretical and Computational Fluid Dynamics*, volume 10, pages 213–237. Springer-Verlag GmbH, January 1998.

[4] A. C. Marta and J. J. Alonso. Toward optimally seeded airflow on hypersonic vehicles using control theory. *Computers & Fluids*, 39(9):1562–1574, October 2010.

[5] A. C. Marta, S. Shankaran, and A. Stein. Blade shape optimization using RANS discrete adjoint solvers. In *Proceedings of the* 2^{nd} *International Conference on Engineering Optimization*, number ENGOPT2010-1410, Lisbon, Portugal, September 2010.

[6] D. X. Wang, L. He, Y. S. Li, R. G. Wells, and T. Chen. Adjoint aerodynamic design optimization for blades in multi-stage turbomachinery: Part II - validation and application. In *Proceedings of the ASME Turbo Expo 2008: Power for Land, Sea and Air*, number GT2008-50209, June 2008.

[7] S. Shankaran and A. C. Marta. Robust optimization for aerodynamic problems using polynomial chaos and adjoints. In *Proceedings of the ASME Turbo Expo 2012: Power for Land, Sea and Air*, number GT2012-69580, Copenhagen, Denmark, June 2012.

[8] D. C. Wilcox. Reassessment of the scale-determining equation for advanced turbulence models. *AIAA Journal*, 26(11):1299–1310, Nov 1998.

[9] M. B. Giles and N. A. Pierce. An introduction to the adjoint approach to design. In *Flow, Turbulence and Combustion*, volume 65, pages 393–415. Kluwer Academic Publishers, 2000.

[10] P. Cusdin and J.-D. Müller. On the performance of discrete adjoint CFD codes using automatic differentiation. *International Journal of Numerical Methods in Fluids*, 47(6–7):939–945, 2005.

[11] A. C. Marta, C. A. Mader, J. R. R. A. Martins, E. van der Weide, and J. J. Alonso. A methodology for the development of discrete adjoint solvers using automatic differentiation tools. *International Journal of Computational Fluid Dynamics*, 21(9–10):307–327, October 2007.

[12] A. C. Marta, S. Shankaran, P. Venugopal, B. Barr, and Q. Wang. Interpretation of adjoint solutions for turbomachinery flows. In *Proceedings of the ASME Turbo Expo 2012: Power for Land, Sea and Air*, number GT2012-69588, Copenhagen, Denmark, June 2012.